

Mobility, Noise Temperature, and Diffusivity of Hot Holes in Germanium

J. P. Nougier and M. Rolland

Laboratoire de Physique des Solides, Centre d'Etudes d'Electronique des Solides, Université des Sciences et Techniques du Languedoc, 34060 Montpellier Cedex, France

(Received 10 November 1972; revised manuscript received 13 April 1973)

Measurements are performed on *p*-type germanium at several temperatures between 77 and 300°K. Mobility is plotted vs electric field up to 10 kV cm⁻¹. Saturation is reached at low temperatures. Critical field E_c and saturation velocity v_s are deduced. E_c varies as $T^{1.93}$ and v_s lies between 8×10^6 and 9×10^6 cm sec⁻¹. An explanation is given to the fact that $\mu(E)/\mu_0$ is found to increase with carrier density. The longitudinal noise temperature $T_{n||}(E)$ is measured vs electric field up to 3 kV cm⁻¹ at different lattice temperatures T in the range 112–300°K. $T_{n||}(E) - T$ varies as $E^{1.6}$ at low field. A flat appears around $E = E_c$. Transverse noise temperature $T_{n\perp}(E)$ is lower than $T_{n||}(E)$. Longitudinal $D_{||}(E)$ and transverse $D_{\perp}(E)$ are deduced. $D_{||}(E)$ is smaller than the Ohmic diffusivity D_0 and reaches $0.15D_0$ at 112°K and 2 kV cm⁻¹. A simple and original iterative method is given for solving the spatially invariant Boltzmann equation in the hot carrier range. Distribution function and transport coefficients are obtained for transitory regime and steady state for *p*-type germanium. The distribution function is never a displaced Maxwellian even at low fields. Comparison with experiment shows that the scattering mechanisms commonly taken into account cannot explain the drift velocity saturation observed experimentally. Multiphonon processes would probably reduce this discrepancy. The relaxation time τ involved in diffusion-coefficient formulas is found to depend on electric field. A formal expression is given for τ .

I. EXPERIMENTAL

Many results in the hot-carrier range deal with conductivity ("first-order" transport coefficient) and have been reported in review papers.¹⁻³ Systematic investigations have been published for silicon.⁴ Second-order transport coefficients, such as noise and diffusion coefficients, have been rarely studied. We report in this paper some results obtained on mobility, noise temperature, and diffusion coefficients in *p*-type germanium. Three samples have been studied:

Sample No. 1: $\rho_{295^\circ\text{K}} = 40 \Omega \text{ cm}$,

$$N_A - N_D = 7.5 \times 10^{13} \text{ cm}^{-3};$$

Sample No. 2: $\rho_{295^\circ\text{K}} = 11.2 \Omega \text{ cm}$,

$$N_A - N_D = 2.6 \times 10^{14} \text{ cm}^{-3};$$

Sample No. 3: $\rho_{295^\circ\text{K}} = 1 \Omega \text{ cm}$,

$$N_A - N_D = 3.5 \times 10^{15} \text{ cm}^{-3}.$$

A. Conductivity

Electric field was applied in $\langle 1\bar{1}0 \rangle$ direction using 2- μ sec pulses at a repetition rate of 1 pulse per 10 sec. Measurements were made with a pulse bridge. Ohmic contacts were obtained by liquid epitaxy.⁵

Relative conductivity $\sigma(E, T)/\sigma_0(T)$ has been studied up to 10 kV cm⁻¹ at different lattice temperatures T between 77 and 300°K. $\sigma(E, T)/\sigma_0(T)$ is identical to the relative mobility $\mu(E, T)/\mu_0(T)$ since the carrier density remains unchanged when applying an electric field: interband induced transi-

tions are assumed to be negligible. Figure 1 shows for sample No. 2 variations versus electric field of

$$E\sigma(E)/\sigma_0 = v_d(E)/\mu_0, \quad (1.1)$$

where $v_d(E)$ is the drift velocity. A good agreement is found at low field with previous results published at 77 and 300°K.⁶⁻¹² However, at high field and low temperature, Fig. 1 clearly exhibits drift-velocity saturation, at 10 kV cm⁻¹ for temperature as high as 143°K. These results bring confirmation of those obtained by Zucker¹¹ and are in dis-

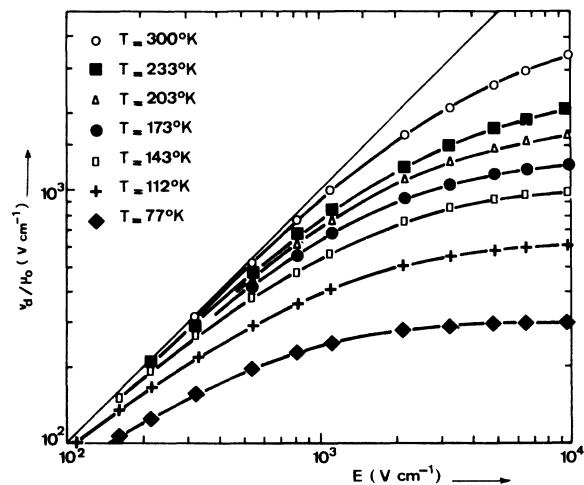


FIG. 1. Ratio of drift velocity v_d to Ohmic mobility μ_0 vs electric field E for sample No. 2.

TABLE I. Measured values of critical field E_c and conductivity σ_c . Saturation velocities v_s have been deduced from μ_0 data of Brown and Bray (Ref. 12).

T ($^{\circ}\text{K}$)	77	112	143	173
E_c (V cm^{-1})	300	610	980	1350
σ_c/σ_0	0.48	0.52	0.54	0.55
v_s (cm sec^{-1})	8.9×10^6	9.0×10^6	8.9×10^6	8.9×10^6

agreement with earlier measurements, among them those of Mendelson and Bray⁷ where the $E^{-0.8}$ law observed at high field was probably due to progressively injecting contacts⁵ since conductivity was higher there than in the present work at high field. Saturation has not yet been observed on p -type silicon.⁴

The critical field E_c defined as

$$E_c = v_s / \mu_0 \quad (1.2)$$

is reported on Table I. The critical conductivity σ_c is defined as

$$\sigma_c = \sigma(E_c). \quad (1.3)$$

σ_c/σ_0 varies slowly with temperature, so that values obtained in Table I can be extrapolated up to 300 $^{\circ}\text{K}$. Results of this extrapolation are given in Table II, as are the corresponding E_c values deduced from σ_c and from curves in Fig. 1. They are in good agreement with extrapolations of curves shown in Fig. 1. Variation of E_c vs T is given in Fig. 2 and shows a $T^{1.93}$ dependence.

Saturation velocities can be obtained by using Eq. (1.2). As μ_0 strongly depends on impurity concentration, μ_0 values obtained by Brown and Bray¹² on similarly doped samples have been used. Results reported in Tables I and II show that v_s varies slowly with temperature and lies between 8×10^6 and 9×10^6 cm sec^{-1} . Similar results have been obtained on silicon.⁴

It must be noted that noninjecting contacts lead to a good variation but wrong values of $\mu(E)/\mu_0$ if contact resistance is not negligible.⁵

The influence of impurity scattering is shown in Fig. 3, where $\mu(E)/\mu_0$ has been plotted versus T at a constant electric field $E = 2 \text{ kV cm}^{-1}$ for sample Nos. 1 and 2. Figure 3 shows that $\mu(E)/\mu_0$ is higher for the more impure sample, in agreement

TABLE II. Extrapolated values of σ_c/σ_0 and E_c .

T ($^{\circ}\text{K}$)	203	233	300
σ_c/σ_0	0.555	0.56	0.567
E_c (V cm^{-1})	1800	2300	4100
v_s (cm sec^{-1})	8.6×10^6	8.3×10^6	8.0×10^6

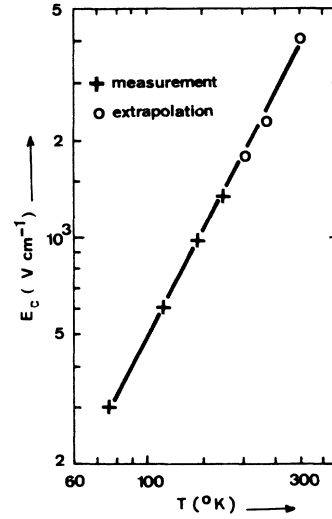


FIG. 2. Characteristic field $E_c = v_s/\mu_0$ vs lattice temperature T for sample No. 2.

with previous experimental results.¹¹ This can be explained as follows: where the electric field is null, the carriers of sample No. 2 are more scattered than those of sample No. 1 and the Ohmic mobilities of the samples are different:

$$\mu_0^{(2)} < \mu_0^{(1)}; \quad (1.4)$$

this is in agreement with previous experimental data.^{12,13} Now, when a sufficiently high electric field is applied, impurity scattering and carrier-carrier scattering are inefficient, and inelastic optical phonon scattering is preeminent and governs mobility; hence

$$\mu^{(2)}(E) \approx \mu^{(1)}(E). \quad (1.5)$$

Equations (1.4) and (1.5) show that

$$\mu^{(2)}(E)/\mu_0^{(2)} > \mu^{(1)}(E)/\mu_0^{(1)}. \quad (1.6)$$

This also explains that the saturation velocity is almost carrier-density independent.³

B. Diffusion Noise Temperature

The results published until now concerning noise-temperature measurements deal with n -type germanium,¹⁴⁻¹⁶ GaAs,¹⁷ n -type silicon,¹⁸ and p -type germanium.^{19,20}

Noise temperatures reported here have been measured at 500 MHz. High-electric-field pulses of 20 μsec duration were applied to the sample along $\langle 110 \rangle$ crystallographic direction. The noise voltage was amplified, then quadratically detected and integrated. When the impedance of the sample was matched to the amplifier the output signal was proportional to the input noise power $k_B(T_n + T_A)$, where T_n and T_A are the noise temperatures of the

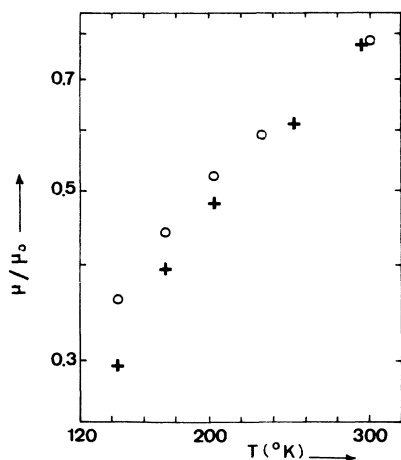


FIG. 3. Variation vs lattice temperature T of relative mobility $\mu(E)/\mu_0$ at $E = 2 \text{ kV cm}^{-1}$ for sample Nos. 1 and 2. +, sample No. $n^\circ 1$; O, sample No. 2.

sample and of the amplifier, and k_B is the Boltzmann constant. T_A and the proportionality factor were determined using a standard noise generator. Details concerning the experimental set up are given in Ref. 5. Temperatures corrections were necessary because of sample heating.

Longitudinal equivalent noise temperature $T_{n\parallel}(E)$ along $\langle 1\bar{1}0 \rangle$ direction has been studied for different

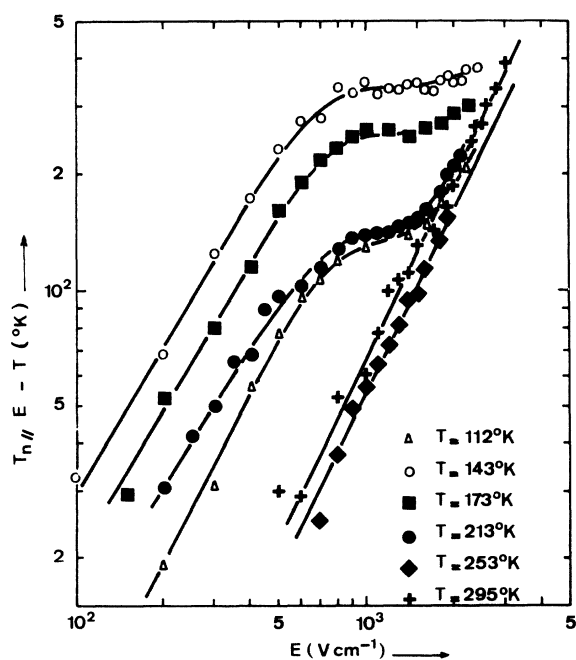


FIG. 4. Longitudinal excess noise temperature $T_{n\parallel}(E) - T$ vs E at different lattice temperatures T for sample No. 1.

lattice temperatures T in the range 112–300 °K. Measurements could not be performed at lower lattice temperatures because contact noise becomes important.⁵ Figure 4 shows, for sample No. 1, excess longitudinal noise temperature $T_{n\parallel}(E) - T$ plotted versus E . It can be seen that at low field (but $E > E_c/10$), $T_{n\parallel}(E) - T$ varies as $E^{1.6}$ at every lattice temperature, and not as E^2 as could be expected from a development in a power series of E .

It must be noted that at lower lattice temperatures, a flat appears in a range of electric field around E_c , and that $T_{n\parallel}(E) - T$ increases again at a higher field. This can be considered as a beginning of experimental confirmation of theory developed in Refs. 21 and 5, following which one can predict

$$\frac{T_{n\parallel}(E)}{T} \approx \frac{D_{\parallel}}{D_0} \frac{E^2}{E_c^2}, \quad \text{where } \frac{E}{E_c} \geq 10, \quad (1.7)$$

where D_{\parallel} and D_0 are longitudinal and Ohmic diffusion coefficients. In practice, Eq. (1.7) leads to a quadratic dependence of $T_{n\parallel}(E)$ vs E for E not exceeding $10E_c$ too much. Unfortunately, the electric field reached was not high enough to exhibit such a variation.

Longitudinal $T_{n\parallel}(E) - T$ and transverse $T_{n\perp}(E) - T$ excess noise temperatures are compared at 300 °K in Fig. 5 for sample No. 3. Longitudinal excess noise is the same as for sample No. 1. It can be seen that the transverse noise temperature is lower than the longitudinal one in agreement with the theory developed in Ref. 21.

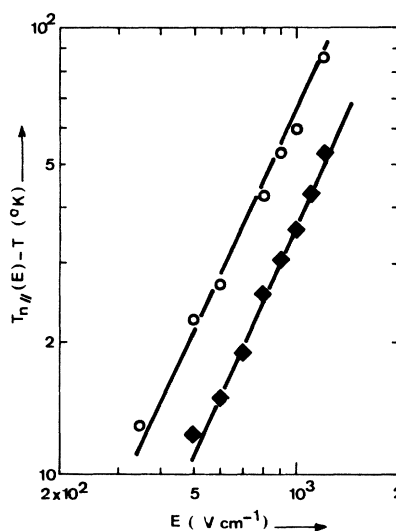


FIG. 5. Comparison between longitudinal $T_{n\parallel}(E) - T$ and transverse $T_{n\perp}(E) - T$ excess noise temperatures at 300 °K for sample No. 3. O, $T_{n\parallel}(E) - T$; ◆, $T_{n\perp}(E) - T$.

C. Diffusion Coefficients

Although important,² diffusion-coefficient measurements for semiconductors in an external electric field are as rare as noise-temperature measurements. However, various techniques can be used and some results have been reported for *n*- and *p*-type germanium,^{19,20} *n*- and *p*-type silicon,²²⁻²⁴ and GaAs.²⁵

Transverse $D_{\perp}(E)$ and longitudinal $D_{\parallel}(E)$ diffusion coefficients in isotropic semiconductors are related to diffusion noise temperatures and mobilities by^{21,26-28}

$$\frac{D_{\perp}(E)}{D_0} = \frac{T_{n\perp}(E)}{T} \frac{\mu(E)}{\mu_0}, \quad (1.8)$$

$$\frac{D_{\parallel}(E)}{D_0} = \frac{T_{n\parallel}(E)}{T} \frac{d}{dE} \frac{v_d(E)}{\mu_0}. \quad (1.9)$$

Relations for semiconductors with anisotropic high mobility are much more complicated.²¹ The validity of Eqs. (1.8) and (1.9) may be assumed for *p*-type germanium. Figure 6 shows variations of $D_{\parallel}(E)/D_0$ for sample No. 1 at different lattice temperatures. It can be seen that $D_{\parallel}(E)/D_0$ is always inferior to unity in the ranges of electric field and temperatures studied. $D_{\parallel}(E)/D_0$ reaches 0.15 at 112 °K and 2 kV cm⁻¹.

$D_{\perp}(E)/D_0$ and $D_{\parallel}(E)/D_0$ are compared at 300 °K in Fig. 7.

II. THEORETICAL

Theoretical studies of electrical-transport coefficients for hot carriers are usually performed by solving the Boltzmann transport equation. Powerful numerical methods have recently been developed, using Monte Carlo techniques²⁹⁻³⁶ as well

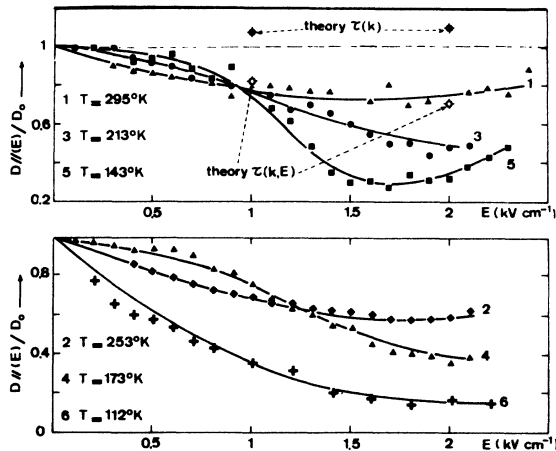


FIG. 6. Experimental $D_{\parallel}(E)/D_0$ vs E at different lattice temperatures T for sample No. 1, compared with theoretical results obtained at 300 °K using a relaxation time $\tau(k)$ defined by Eq. (2.3) or $\tau(k, E)$ defined by Eq. (2.29).

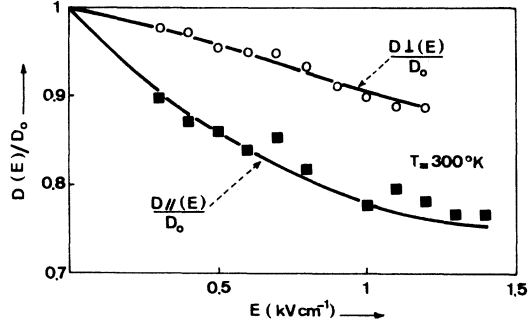


FIG. 7. Comparison between $D_{\parallel}(E)/D_0$ and $D_{\perp}(E)/D_0$ at 300 °K for sample No. 1.

as iterative techniques.³⁷⁻⁴⁵ An original iterative method will be presented (Sec. II A). It will be applied to *p*-type germanium, within the hypothesis commonly made for this material. Transitory and stationary distribution functions will be studied (Sec. II B) as well as the corresponding electrical transport coefficients (Sec. II C). Diffusivity will be studied in a separate section (Sec. II D). Theoretical results will be compared to experimental ones of the present work.

A. Numerical Resolution of the Boltzmann Equation

1. Method

A semiconductor in thermodynamic equilibrium at temperature T at time $t \leq 0$ is acted on at $t > 0$ by a constant homogeneous field force \vec{F} . The carrier distribution function $f(\vec{k}, \vec{F}, t)$ is then solution of the homogeneous Boltzmann equation

$$\frac{\partial f(\vec{k}, \vec{F}, t)}{\partial t} = -\frac{1}{\hbar} \vec{F} \cdot \nabla_{\vec{k}} f(\vec{k}, \vec{F}, t) + \hat{C} f(\vec{k}, \vec{F}, t) = \psi f(\vec{k}, \vec{F}, t), \quad (2.1)$$

where \hat{C} is the collision operator

$$\hat{C} f(\vec{k}, \vec{F}, t) = \sum_{\vec{k}'} [f(\vec{k}', \vec{F}, t) P(\vec{k}' - \vec{k}) - \frac{f(\vec{k}, \vec{F}, t)}{\tau(\vec{k})}], \quad (2.2)$$

where $P(\vec{k} - \vec{k}')$ is the transition probability per unit time from state \vec{k} to state \vec{k}' , and $\tau(\vec{k})$ is the relaxation time defined as

$$[\tau(\vec{k})]^{-1} = \sum_{\vec{k}'} P(\vec{k} - \vec{k}'). \quad (2.3)$$

Summation over states \vec{k}' can be transformed into integral in $\{\vec{k}\}$ space. The validity of Eqs. (2.1)–(2.3) will not be discussed here (for this see Refs. 46–49, for instance). The initial condition is given by

$$f(\vec{k}, \vec{F}, t=0) = f_0(\epsilon), \quad (2.4)$$

where $f_0(\epsilon)$ is the carrier thermodynamic-equilibrium distribution function.

Equations (2.1) and (2.2) assume that operator ψ does not depend on time and acts only in $\{\vec{k}\}$ space. Let us suppose that $f(\vec{k}, \vec{F}, t)$ is known at some instant t . Then application of operator ψ_2 gives $\partial f(\vec{k}, \vec{F}, t)/\partial t$ at this time. Derivation of equation (2.1) with respect to the time leads to

$$\frac{\partial^2 f(\vec{k}, \vec{F}, t)}{\partial t^2} = \psi \left(\frac{\partial f(\vec{k}, \vec{F}, t)}{\partial t} \right). \quad (2.5)$$

This gives $\partial^2 f(\vec{k}, \vec{F}, t)/\partial t^2$ by application of operator ψ to the just-calculated function $\partial f(\vec{k}, \vec{F}, t)/\partial t$. Hence, successive derivatives of $f(\vec{k}, \vec{F}, t)$ with respect to t can be calculated. This gives the distribution function at time $t + \Delta t$ if one supposes that f is developable in a power series of Δt ,

$$f(\vec{k}, \vec{F}, t + \Delta t) = \sum_{n=0}^{\infty} \frac{(\Delta t)^n}{n!} \frac{\partial^n f(\vec{k}, \vec{F}, t)}{\partial t^n}. \quad (2.6)$$

Since $f(\vec{k}, \vec{F}, t=0)$ is known by Eq. (2.4), one can calculate $f(\vec{k}, \vec{F}, t)$ at times $\Delta t, 2\Delta t, \dots$, that is the evolution with time of the distribution function and hence of all the mean values associated to it. If $\phi(\vec{k})$ is some function of state \vec{k} , one gets

$$\phi(t) = \langle \phi(\vec{k}) \rangle = \sum_{\vec{k}} \phi(\vec{k}) f(\vec{k}, \vec{F}, t). \quad (2.7)$$

After a time t_{st} , the stationary state is reached. In theory it can be obtained directly if t is set to be equal to zero and $\Delta t = t_{st}$ in Eq. (2.6).

In practice, only a finite number of derivatives can be calculated:

$$f(\vec{k}, \vec{F}, t + \Delta t) \approx \sum_{n=0}^p \frac{(\Delta t)^n}{n!} \frac{\partial^n f(\vec{k}, \vec{F}, t)}{\partial t^n} \quad (2.8)$$

Therefore, Δt must be much smaller than t_{st} and a number of iterations are necessary to reach the stationary state.

This method can also be applied for solving non-homogeneous integrodifferential equations of the type

$$\frac{\partial f(\vec{k}, \vec{F}, t)}{\partial t} - \psi f(\vec{k}, \vec{F}, t) = f_1(\vec{k}, \vec{F}, t), \quad (2.9)$$

where $f_1(\vec{k}, \vec{F}, t)$ is some known function. This allows, for instance, solving perturbed Boltzmann equations.

The case of time-dependent field force $\vec{F}(t)$ can be solved by using the same technique. Then in partial derivation of Eq. (2.1), with respect to the time, appears the known function $-(1/\hbar) \times [d\vec{F}(t)/dt] \cdot \vec{\nabla}_k f(\vec{k}, \vec{F}, t)$ in addition to the second member of Eq. (2.5).

In principle, no limitation appears with regard to energy-band shapes.

2. Effective Calculation for *p*-Type Germanium

The method just described has been applied to *p*-type germanium in a high electric field \vec{E} . Hence

$$\vec{F} = q\vec{E}. \quad (2.10)$$

The usual assumptions concerning this material have been made, namely, (i) one kind of combined heavy and light holes; (ii) spherical parabolic energy-band surface centered at $k=0$; (iii) interactions of the carriers with both acoustical and nonpolar-optical phonons; (iv) effective deformation potentials; and (v) phonons in thermodynamic equilibrium.

Spherical coordinates have been chosen with polar axis along \vec{E} . A combined heavy- and light-hole effective mass $m = 0.36m_0$ leads to

$$D_{PA} = 4.34 \text{ eV}, \quad \Xi_0 = 0.886 \times 10^9 \text{ eV cm}^{-1}, \quad (2.11)$$

where D_{PA} and Ξ_0 are the effective acoustic deformation potential and optical deformation field.

$\{\vec{k}\}$ space was divided into 320 or 480 meshes: 16 steps for θ varying from 0 to π ($\Delta\theta = \frac{1}{16}\pi$); 20 or 30 steps for k ($\Delta k = 10^9 \text{ m}^{-1}$); k varying from 0 to 2×10^9 or $3 \times 10^9 \text{ m}^{-1}$. Between 20 and 150 iterations were necessary to reach stationarity, t_{st} varying with T and E . If t_{on} is the time necessary for drift velocity to reach its maximum value ($t_{on} \leq t_{st}$), Δt is generally taken to be equal to $\frac{1}{10} t_{on}$ or $\frac{1}{20} t_{on}$. t_{st} lies between 2.5×10^{-12} and 1.5×10^{-11} sec according to the T and E domain. Derivatives with respect to k and θ were calculated by approximating f by a sixth-order polynomial at each point except near the edge of the $\{\vec{k}\}$ domain.

Five derivatives were used at each time step [$p=5$ in Eq. (2.8)]. Calculations were performed on an IBM 360.40. About 50 000 bytes were used. Twenty-three seconds were necessary to perform one iteration. The computing time necessary to reach stationarity was between 10 and 60 min. Further details are given in Ref. 5.

B. Distribution Function

Evolution with time between 0 and t_{st} of the distribution function along electric field, namely,

$$f(k, k_z=0, E, t) = f(k, \theta = \begin{cases} 0 \\ \pi \end{cases}, E, t) \quad (2.12)$$

is shown at 300 °K and 20 kV cm⁻¹ in Fig. 8. \vec{k}_d is the wave vector associated with stationary drift velocity \vec{v}_d ; it can be seen that the distribution function spreads in $\{\vec{k}\}$ space and is driven along electric field while its maximum decreases. Similar results had been obtained.^{41,44}

Stationary distribution functions along electric field are shown at 300 and 77 °K in Fig. 9. A curve obtained at 20 kV cm⁻¹ and 300 °K shows the

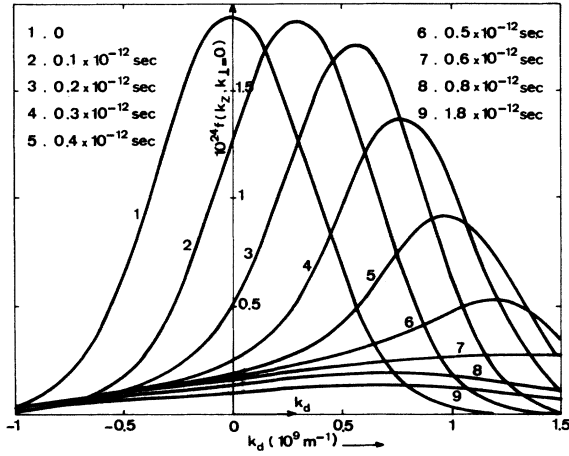


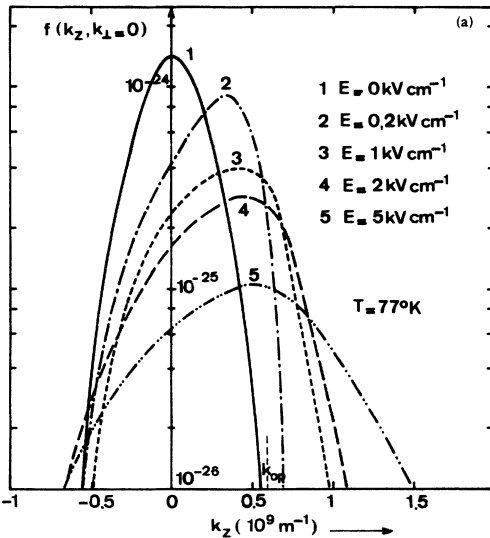
FIG. 8. Time evolution of the distribution function along k_x at $T=300^\circ\text{K}$ and $E=20\text{ kV cm}^{-1}$.

necessity of exploring the $\{\vec{k}\}$ space as far as $k=3\times 10^9\text{ m}^{-1}$. k_{op} is the wave vector associated with the optical-phonon energy $\epsilon_{op}=\hbar^2 k_{op}^2/2m$. Figure 9 shows that $f(\vec{k}, \vec{E})$ is not symmetric and therefore cannot be identified to a displaced Maxwellian even at low field. $f(\vec{k}, \vec{E})$ can be expanded in Legendre polynomials

$$f(\vec{k}, \vec{E})=f(k, \theta, E)=\sum_{l=0}^{\infty} g_l(k, E)P_l(\cos\theta). \quad (2.13)$$

$g_l(k, E)$ is obtained by a simple integration

$$g_l(k, E)=\frac{2l+1}{2} \times \int_0^\pi P_l(\cos\theta) f(k, \theta, E) \sin\theta d\theta. \quad (2.14)$$



It was found that $g_0(\epsilon)$ could be identified with two Maxwellian functions intersecting in the vicinity of ϵ_{op} , in agreement with previous results.^{29,37,38} Figure 10 shows variations of $g_2(\epsilon)/g_0(\epsilon)$ at $T=77^\circ\text{K}$; it can be seen that neglecting $g_2(\epsilon)$ can be justified at low field but not at a higher field, in agreement with experimental results.^{50,51} Moreover, Fig. 12 shows that at high-field anisotropy decreases since $g_2(\epsilon)/g_0(\epsilon)$ diminishes.

C. Transport Coefficients

1. Drift Velocity

Ohmic mobility μ_0 is given by

$$\mu_0=\frac{\hbar^2 q}{3\pi^2 m k_B T} \int_0^\infty \tau(k) f_0(k) k^4 dk, \quad (2.15)$$

where k_B is the Boltzmann constant. $\tau(k)$ and $f_0(k)$ are defined by Eqs. (2.3) and (2.4).

Drift velocity $v_d(t)$ is given by

$$v_d(t)=\frac{\hbar}{2\pi^2 m} \int_0^\pi d\theta \int_0^\infty dk f(k, \theta, E, t) \times k^3 \cos\theta \sin\theta. \quad (2.16)$$

Time evolutions are shown in Fig. 11. Agreement with previous theoretical result⁴⁴ is excellent.

Theoretical variations of $v_d(E)/\mu_0$ are plotted versus E in Fig. 12 and are compared with experimental results of the present work (Sec. I A) at 300, 173, and 77°K . At 77°K discrepancy between experiment and theory can be explained at low field by impurity scattering as can be deduced from Fig. 3. However at higher fields the slope of theoretical $\mu(E)/\mu_0$ is approximately -0.8 while the experi-

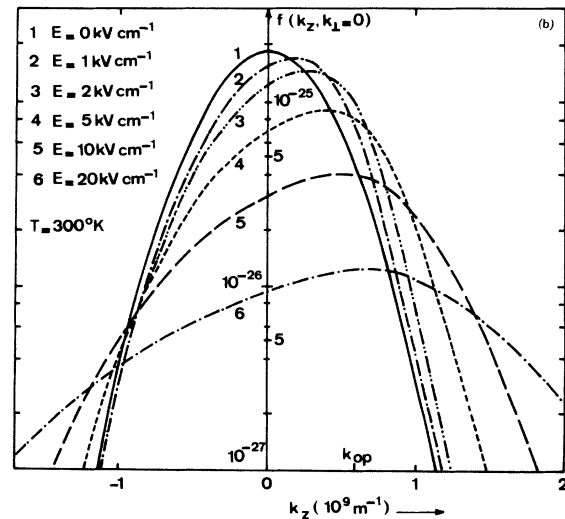
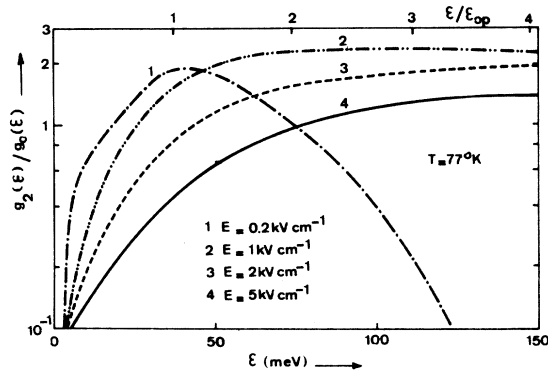


FIG. 9. Stationary distribution function along k_x for different electric field intensities; (a) at $T=77^\circ\text{K}$, (b) at $T=300^\circ\text{K}$.

FIG. 10. Ratio $g_2(\epsilon)/g_0(\epsilon)$ vs energy ϵ .

mental slope is -1 . This discrepancy is substantiated by the fact that v_d/μ_0 becomes superior to experimental $E_c = v_s/\mu_0$ even at high temperatures. Comparisons between theory and experiment are reported in Table III for equivalent fields, namely, $E = 5E_c$, at 77, 173, and 300 °K. It can be seen that theoretical values of $v_d(E = 5E_c)/\mu_0$ are superior to the corresponding experimental values of E_c at 173 and 300 °K, and hardly reach $\frac{2}{3} E_c$ at 77 °K. This brings evidence that discrepancy between theory and experiment increases with increasing temperature and electric field.

Now impurity scattering is negligible at high temperatures. We shall show in the following that assuming multiple-phonon scattering may reduce discrepancy between theory and experiment. In multiple-phonon scattering a carrier of energy greater than $2\epsilon_{op}$ can emit more than one optical

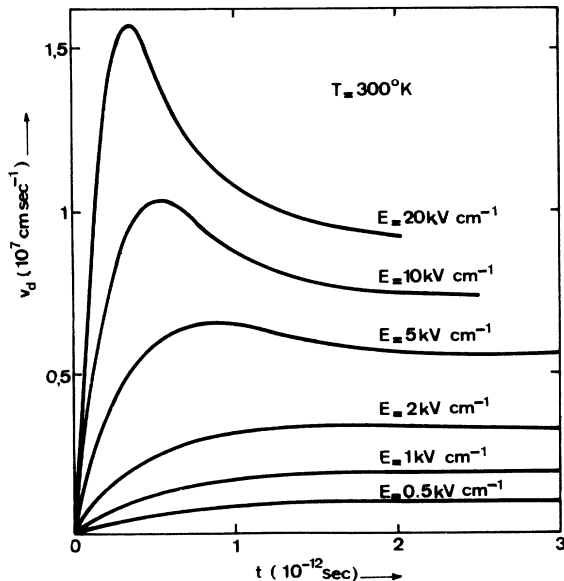
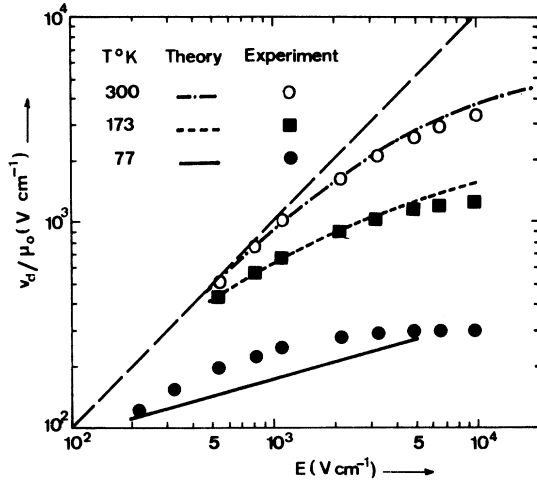


FIG. 11. Time evolution of drift velocity at 300 °K.

FIG. 12. Ratio $v_d(E)/\mu_0$ vs E ; comparison between theoretical and experimental results for sample No. 2.

phonon. So this mechanism allows a greater energy relaxation of the carriers, that is, diminishes the volume of the domain in $\{\vec{k}\}$ space where the distribution function is not negligible. It can then be expected that multiple-phonon scattering lowers all mean values, among them the drift velocity. The proportion of carriers per unit volume having energy comprised between ϵ and $\epsilon + d\epsilon$, namely, $n(\epsilon)d\epsilon/N$, can be easily evaluated. N is the number of carriers per unit crystal volume

$$\frac{n(\epsilon)}{N} = \frac{1}{2\pi^2} \left(\frac{2m}{\hbar^2} \right)^{3/2} \epsilon^{1/2} g_0(\epsilon). \quad (2.17)$$

$n(\epsilon)/N$ curves are shown in Fig. 13. Integration of Eq. (2.17) over ϵ between $2\epsilon_{op}$ and infinity gives the proportion of carriers enabling multiple-phonon processes. Some results are reported in Table IV, and show, for example, that for $E = 5E_c$ the proportion of carriers able to emit two phonons is less than 7% at 77 °K and reaches 85% at 300 °K. Therefore, neglecting multiphonon processes leads to an error that increases with temperature and with electric field intensity. So this scattering mechanism appears as an *a priori* possibility of reducing discrepancy between theory and experiment as regards drift-velocity saturation. How-

TABLE III. Comparison between experimental $E_c = v_s/\mu_0$ and theoretical $v_d(5E_c)/\mu_0$.

T (°K)	77	173	300
E_c (V cm ⁻¹)	300	1350	4100
Experimental			
$v_d(5E_c)/\mu_0$ (V cm ⁻¹)			
Theoretical	195	1400	4600

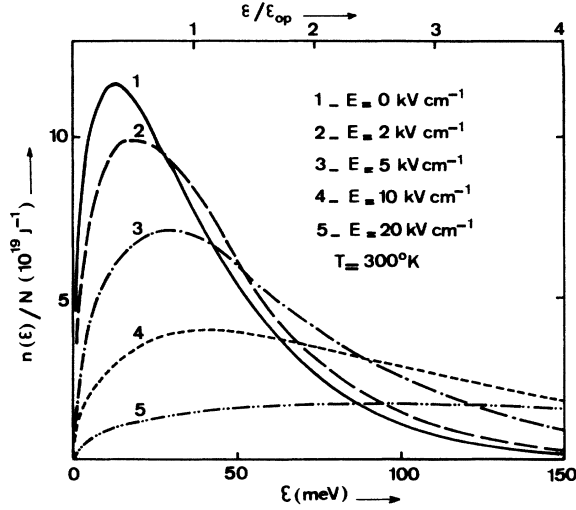


FIG. 13. Relative carriers density per unit energy $n(\epsilon)/N$ vs energy ϵ .

ever, this discrepancy may be also due to the failure of some of the hypothesis checked in Sec. II A 2.

2. Mean Energy

The mean energy is given by

$$\epsilon(t) = \frac{\hbar^2}{4\pi^2 m} \int_0^\pi d\theta \int_0^\infty dk f(k, \theta, E, t) \times k^4 \sin\theta. \quad (2.18)$$

In transitory regime, $\epsilon(t)$ was never found to overshoot its stationary value. Root-mean-square velocity v_{rms} can be derived from energy using the relation

$$v_{\text{rms}} = (\langle v^2 \rangle)^{1/2} = (2\epsilon/m)^{1/2}. \quad (2.19)$$

Figure 14 shows theoretical variations of stationary v_d/v_{rms} vs E at 77, 173, and 300 °K, compared with experimental results of Bray and Pinson.⁵¹ Agreement is good beyond 0.5 kV cm⁻¹; discrepancy below is perhaps due to impurity scattering, since experiments were performed on doped samples ($N_D - N_A = 5.7 \times 10^{15}$ cm⁻³).

D. Diffusivity

1. Definitions and Expressions

Very sparse theoretical results for diffusion coefficients^{24,33,45,52} have been obtained till now, in spite of numerous solutions of the Boltzmann equation mentioned in Sec. I.

Element $D_{\alpha\beta}(\vec{E})$ of diffusivity tensor $\vec{D}(\vec{E})$ is defined⁵³ as

$$D_{\alpha\beta}(E, \nu) = \int_0^\infty \cos 2\pi\nu t' \times \langle [v_\alpha(t) - v_{d\alpha}] [v_\beta(t+t') - v_{d\beta}] \rangle dt', \quad (2.20)$$

TABLE IV. Theoretical proportions of carriers in which energy is superior to $2\epsilon_{\text{op}}$ at 77 and 300 °K for some electric field intensities.

E (kV cm ⁻¹)	0	0.2	1	2	5	10	20
$T = 300$ °K	0.13	0.14	0.32	0.59	0.85
$T = 77$ °K	≈ 0	≈ 0	0.02	0.07	0.35

where $v_\alpha(t)$ is the component along the α direction of a carrier instantaneous velocity. Equation (2.20) yields,^{21,26} in stationary regime at usual frequencies,

$$D_\perp(E) = \frac{\hbar^2}{4\pi^2 m^2} \int_0^\pi d\theta \int_0^\infty dk \tau(k, \theta, E) \times f(k, \theta, E) k^4 \sin^3\theta, \quad (2.21)$$

$$D_\parallel(E) = \frac{1}{2\pi^2} \int_0^\pi d\theta \int_0^\infty dk \tau(k, \theta, E) \times \left(\frac{\hbar k}{m} \cos\theta - v_d \right)^2 f(k, \theta, E) k^2 \sin\theta. \quad (2.22)$$

$D_\perp(E)$ and $D_\parallel(E)$ are transverse and longitudinal diffusion coefficients measured experimentally. $\tau(\vec{k}, \vec{E}) = \tau(k, \theta, E)$ is the relaxation time.

2. Formal Expression for Relaxation Time

Relaxation time $\tau(\vec{k}, \vec{F})$ can be defined as being the time necessary for a system in a field force \vec{F} to come back to its stationary state after a small perturbation.

Hence, let us suppose that at time $t < 0$, the system is acted upon by a field force $\vec{F} + \delta\vec{F}$ and is defined by its stationary distribution function $f(\vec{k}, \vec{F} + \delta\vec{F})$. If, at time $t = 0$, the perturbation $\delta\vec{F}$ is removed, the instantaneous distribution function is $f(\vec{k}, \vec{F}, t)$ and evolves towards

$$f(\vec{k}, \vec{F}) = \lim_{t \rightarrow \infty} f(\vec{k}, \vec{F}, t). \quad (2.23)$$

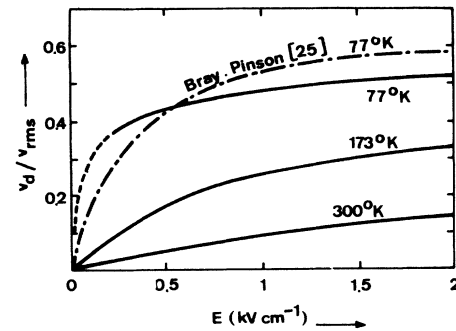


FIG. 14. Ratio of drift velocity v_d to root-mean-square velocity v_{rms} vs electric field at different temperatures and comparison with experimental results (Ref. 25).

$\tau(\vec{k}, \vec{F})$ is then defined as

$$\begin{aligned} & \left(\frac{\partial f(\vec{k}, \vec{F}, t)}{\partial t} \right)_{t=0} \\ &= \lim_{|\delta \vec{F}| \rightarrow 0} \left(- \frac{f(\vec{k}, \vec{F} + \delta \vec{F}) - f(\vec{k}, \vec{F})}{\tau(\vec{k}, \vec{F})} \right). \end{aligned} \quad (2.24)$$

Now $f(\vec{k}, \vec{F}, t)$ is the solution of the time-dependent Boltzmann equations

$$\frac{\partial f(\vec{k}, \vec{F}, t)}{\partial t} + \frac{1}{\hbar} \vec{F} \cdot \vec{\nabla}_{\vec{k}} f(\vec{k}, \vec{F}, t) = \hat{C} f(\vec{k}, \vec{F}, t), \quad (2.25)$$

$$f(\vec{k}, \vec{F}, t=0) = f(\vec{k}, \vec{F} + \delta \vec{F}); \quad (2.26)$$

and $f(\vec{k}, \vec{F} + \delta \vec{F})$ is the solution of

$$(1/\hbar)(\vec{F} + \delta \vec{F}) \cdot \vec{\nabla}_{\vec{k}} f(\vec{k}, \vec{F} + \delta \vec{F}) = \hat{C} f(\vec{k}, \vec{F} + \delta \vec{F}). \quad (2.27)$$

Equation (2.25) gives, at $t=0$, taking into account (2.26) and (2.27),

$$\left(\frac{\partial f(\vec{k}, \vec{F}, t)}{\partial t} \right)_{t=0} = \frac{1}{\hbar} \delta \vec{F} \cdot \vec{\nabla}_{\vec{k}} f(\vec{k}, \vec{F} + \delta \vec{F}). \quad (2.28)$$

Finally, Eqs. (2.24) and (2.28) lead to

$$\tau(\vec{k}, \vec{F}) = \lim_{|\delta \vec{F}| \rightarrow 0} \frac{-\hbar \delta \vec{F} \cdot \vec{\nabla}_{\vec{k}} f(\vec{k}, \vec{F})}{\delta \vec{F} \cdot \vec{\nabla}_{\vec{k}} f(\vec{k}, \vec{F})}. \quad (2.29)$$

It can be easily shown that

$$\lim_{|\vec{F}| \rightarrow 0} \tau(\vec{k}, \vec{F}) = \tau(\vec{k}), \quad (2.30)$$

where $\tau(\vec{k})$ is given by Eq. (2.3).

3. Numerical Results

Longitudinal and transverse diffusion coefficients were computed using formulas (2.21) and (2.22). $\tau(\vec{k}, \vec{F})$ was calculated following Eq. (2.29); $\delta \vec{F} \cdot \vec{\nabla}_{\vec{k}} f(\vec{k}, \vec{F})$ was approximated by

$$\delta \vec{F} \cdot \vec{\nabla}_{\vec{k}} f(\vec{k}, \vec{F}) \simeq f(k, \theta, E + \delta E) - f(k, \theta, E), \quad (2.31)$$

where δE was taken equal to $\frac{5}{100} E$.

Figure 6 shows the comparison between theoretical $D_{11}(E)/D_0$ and experimental results for sample No. 1 at 300°K. Computation was performed using $\tau(\vec{k}, \vec{F})$ defined by Eq. (2.29) as well as the commonly used^{23,26} $\tau(\vec{k})$ given by Eq. (2.3). Figure 15 shows comparison between experimental and theoretical results obtained at 1 kV cm⁻¹ for different lattice temperatures. Figures 6 and 15 prove that the relaxation time actually depends on electric field and is given by formula (2.29). Unfortunately, singularity 0/0 occurs for a set of \vec{k} values for which $\delta \vec{F} \cdot \vec{\nabla}_{\vec{k}} f(\vec{k}, \vec{F}) = 0$ in Eq. (2.29); this singularity could not be removed by the authors and can be shown⁵ to introduce drastic errors in the computation of $D_{11}(E)$ at high fields and of $D_{\perp}(E)$ at low and intermediate fields, so that theoretical and experimental results of $D_{\perp}(E)$ could not be usefully compared.

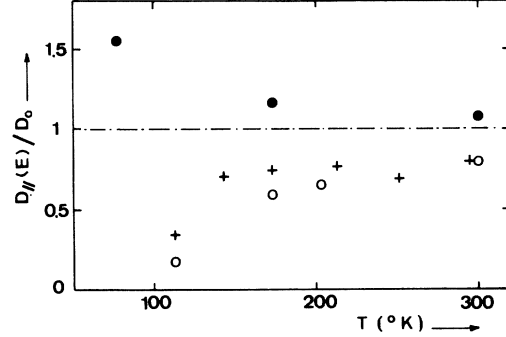


FIG. 15. Comparison between theoretical and experimental $D_{11}(E)/D_0$ at $E=1$ kV cm⁻¹ for different lattice temperatures T . +, Experiment (sample No. 1); ○, theory with $\tau=\tau(\vec{k}, E)$ defined by Eq. (2.29); ●, theory with $\tau=\tau(\vec{k})$ defined by Eq. (2.3).

III. CONCLUSION

A new and simple iterative method was elaborated for numerically solving the spatially invariant Boltzmann equation in the hot carrier range. No limitation appears with regard to energy-band shapes or scattering mechanisms. This method was applied to p -type germanium within the hypothesis commonly made for this material.

Evolution with time of the distribution function was found to be in agreement with other theoretical results obtained by different methods. The stationary distribution function $f(\vec{k}, \vec{E})$ was never found to be a displaced Maxwellian, even at low field. It was shown that $g_2(\epsilon)$ could not be neglected at intermediate field, in agreement with other experimental work, and that anisotropy of $f(\vec{k}, \vec{E})$ diminishes at high field.

A set of experimental conductivity curves obtained with the same sample up to 10 kV cm⁻¹ at different temperatures lying between 77 and 300°K brought evidence that drift velocity reaches saturation at high field. Critical field E_c and saturation velocity v_s were, for the first in p -type germanium, plotted versus temperature; E_c was found to vary as $T^{1.93}$; v_s remains almost constant. $\mu(E)/\mu_0$ was found to increase with carrier density and this variation could be explained. A careful comparison between theoretical and experimental results of the present work brings evidence that the fit is good at low field and that a strong discrepancy occurs at high field and high temperature, which proves the failure of some of the hypotheses concerning the relaxation processes of the carriers in p -type germanium. It was shown that assuming multiphonon scattering could reduce the observed discrepancy.

Experimental noise temperature and diffusivity versus electric field were obtained for the first

time for a set of temperatures below 300 °K on the same sample. Unfortunately, measurements could not be performed below 112 °K. Experimental curves show that excess noise temperature varies as $E^{1.6}$ at weak field, variation becoming more complicated at higher field according to.²¹ Comparison between experimental and theoretical results proved that the relaxation time $\tau(k, E)$ involved in diffusion coefficients actually depend on electric field and that the expression (2.29) given for $\tau(k, E)$ is correct. It must be noted that the

relaxation-time hypothesis is merely an approximation, since correlations between observables involve operators and not scalars; however, such an approximation may be useful as long as a more elaborate expression for velocity correlation is not obtained.

ACKNOWLEDGMENTS

The authors are much indebted to Professor M. Savelli who started this research and to M. J. R. Galéa who programmed the numerical calculations.

- ¹E. G. S. Paige, *Progress in Semiconductors* (Heywood, London, 1964), Vol. 8.
- ²E. M. Conwell, *Solid State Physics* (Academic, New York, 1967), Suppl. 9.
- ³M. Asche and O. G. Sarbei, *Phys. Status Solidi* **33**, 9 (1969).
- ⁴C. Canali, G. Ottaviani, and A. Quaranta Alberigi, *J. Phys. Chem. Solids* **32**, 1707 (1971).
- ⁵J. P. Nougier, thèse de Doctorat ès Sciences (Montpellier, Fré, 1972) (unpublished).
- ⁶E. J. Ryder, *Phys. Rev.* **90**, 766 (1953).
- ⁷K. S. Mendelson and R. Bray, *Proc. Phys. Soc. Lond. B* **70**, 899 (1957).
- ⁸R. D. Larrabee, *J. Appl. Phys.* **30**, 857 (1959).
- ⁹A. C. Prior, *J. Phys. Chem. Solids* **12**, 175 (1959).
- ¹⁰K. Seeger, *Phys. Rev.* **114**, 476 (1959).
- ¹¹J. Zucker, *J. Phys. Chem. Solids* **12**, 350 (1960).
- ¹²D. M. Brown and R. Bray, *Phys. Rev.* **127**, 1593 (1962).
- ¹³C. Goldberg, E. N. Adams, and R. E. Davis, *Phys. Rev.* **105**, 863 (1957).
- ¹⁴E. Erlbach and J. B. Gunn, *Phys. Rev. Lett.* **8**, 280 (1962).
- ¹⁵E. Erlbach and J. B. Gunn, *Proceedings of the International Conference on Semiconductors Exeter, 1962*, edited by A. C. Stikland (The Institute of Physics and The Physical Society, London, 1962), p. 128.
- ¹⁶L. G. Hart, *Can. J. Phys.* **48**, 531 (1970).
- ¹⁷C. A. Bryant, *Bull. Am. Phys. Soc.* **9**, 62 (1964).
- ¹⁸Yu. K. Pozhela, V. A. Bareikis, and I. B. Matulenene, *Sov. Phys.-Semicond.* **2**, 503 (1968).
- ¹⁹V. A. Bareikis, I. B. Vaitkevichyute, and K. Pozhela, *Liet. Fiz. Rinkiny* **6**, 437 (1966).
- ²⁰V. Bareikis, K. Pozhela, I. B. Matulenene, in *Proceedings of the Ninth International Conference on the Physics of Semiconductors*, edited by S. M. Ryvkin (Nauka, Leningrad, 1968), p. 760.
- ²¹J. P. Nougier, *Physica (Utr.)* **64**, 209 (1973).
- ²²T. W. Sigmon, and J. F. Gibbons, *Appl. Phys. Lett.* **15**, 320 (1969).
- ²³G. Persky and D. J. Bartelink, *Phys. Rev. B* **1**, 1614 (1970).
- ²⁴G. Persky and D. J. Bartelink, *J. Appl. Phys.* **42**, 4414 (1971).
- ²⁵J. G. Ruch and G. S. Kino, *Phys. Rev.* **174**, 921 (1968).
- ²⁶P. J. Price, *IBM J. Res. Dev.* **3**, 191 (1959).
- ²⁷P. J. Price, in *Fluctuation Phenomena in Solids*, edited by R. E. Burgess (Academic, New York, 1965), Chap. 8.
- ²⁸V. L. Gurevitch, *Zh. Eksp. Teor. Fiz.* **43**, 1771 (1962) [*Sov. Phys.-JETP* **16**, 1252 (1963)].
- ²⁹T. Kurosawa, *J. Phys. Soc. Jap. Suppl.* **21**, 424 (1966).
- ³⁰J. G. Ruch and G. S. Kino, *Phys. Rev.* **174**, 921 (1968).
- ³¹A. D. Boardman, W. Fawcett, and N. D. Rees, *Solid State Commun.* **6**, 305 (1968).
- ³²W. Fawcett and J. G. Ruch, *Appl. Phys. Lett.* **15**, 368 (1969).
- ³³W. Fawcett and H. D. Rees, *Phys. Lett. A* **29** 578 (1969).
- ³⁴W. Fawcett, *Proceedings of the International Conference on the Physics of Semiconductors*, Cambridge, Mass., 1970, p. 51 (unpublished).
- ³⁵W. Fawcett, A. D. Boardman, and S. Swain, *J. Phys. Chem. Solids* **31**, 1963 (1970).
- ³⁶W. Fawcett and E. G. S. Paige, *J. Phys. C* **4**, 1801 (1971).
- ³⁷H. F. Budd, *J. Phys. Soc. Jap. Suppl.* **21**, 420 (1966).
- ³⁸H. F. Budd, *Phys. Rev.* **158**, 798 (1967).
- ³⁹P. J. Price, in Ref. 20, Vol. 2, p. 753.
- ⁴⁰H. D. Rees, *Phys. Lett. A* **26**, 416 (1968).
- ⁴¹H. D. Rees, *J. Phys. Chem. Solids* **30**, 643 (1969).
- ⁴²H. D. Rees, *IBM J. Res. Dev.* **13**, 537 (1969).
- ⁴³P. C. Kwok and T. D. Schultz, *Phys. Rev. B* **3**, 1180 (1971).
- ⁴⁴P. A. Lebwohl and P. M. Marcus, *Solid State Commun.* **9**, 1671 (1971).
- ⁴⁵P. A. Lebwohl and P. J. Price, *Solid State Commun.* **9**, 1221 (1971).
- ⁴⁶M. Dresden, *Rev. Mod. Phys.* **33**, 265 (1961).
- ⁴⁷*Solid State Physics*, Suppl. 4, edited by A. C. Beer (Academic, New York, 1963).
- ⁴⁸R. Balescu, *Physica (Utr.)* **27**, 693 (1961).
- ⁴⁹P. N. Argyres, *Lectures in Theoretical Physics* (Interscience, New York, 1965), Vol. 8a.
- ⁵⁰A. C. Baynham, and E. G. S. Paige, *Phys. Lett.* **6**, 7 (1963).
- ⁵¹R. Bray and W. E. Pinson, *Phys. Rev. Lett.* **11**, 268 (1963).
- ⁵²Patrick Hu and P. J. Price, *IBM Research Report No. NW-18* (1967) (unpublished).
- ⁵³W. Shockley, J. A. Copeland, and R. P. James, *Quantum Theory of Atoms, Molecules and the Solid State*, edited by P. O. Lowdin (Academic, New York, 1966), p. 537.